Real-time Nowcasting and Forecasting of COVID-19 Dynamics in England: the first wave?

Paul Birrell,[1,2] Joshua Blake[2], Edwin van Leeuwen[1], PHE Joint Modelling Cell, Nick Gent[3], Daniela De Angelis[2,1]

[1]National Infection Service, Public Health England, 61 Colindale Avenue, NW9 5HT, UK
[2]MRC Biostatistics Unit, University of Cambridge Institute of Public Health, Cambridge Biomedical Campus, CB2 0SR, UK
[3]Emergency Response Department, Public Health England, Porton Down, SP4 0JG, UK

24th August 2020

England has been heavily affected by the SARS-CoV-2 pandemic, with severe 'lock-down' mitigation measures now gradually being lifted. The real-time pandemic monitoring presented here has contributed to the evidence informing this pandemic management. Estimates on the 10th May showed lock-down had reduced transmission by 75%, the reproduction number falling from 2.6 to 0.61. This regionally-varying impact was largest in London of 81% (95% CrI: 77%–84%). Reproduction numbers have since slowly increased, and on 19th June the probability that the epidemic is growing was greater than 5% in two regions, South West and London. An estimated 8% of the population had been infected, with a higher proportion in London (17%). The infection-to-fatality ratio is 1.1% (0.9%–1.4%) overall but 17% (14%–22%) among the over-75s. This ongoing work will be key to quantifying any widespread resurgence should accrued immunity and effective contact tracing be insufficient to

preclude a second wave.

1 Introduction

Since the 31st of December 2019, when the government of Wuhan reported treating cases of pneumonia of unknown cause (*1*), more than 13 million individuals have been reported as being infected by SARS-COV-2 globally and over 500,000 have died (*2*). Spread of SARS-COV-2 from Wuhan to other Chinese provinces, Thailand, Japan and the Republic of Korea rapidly occurred in the first 3 weeks of January 2020 (*3*), with an early incursion into Europe centred around clusters in Bavaria, Germany and Haute-Savoie, France, both linked to subsequent cases in Spain (*4*). This international spread eventually led the World Health Organisation to declare a pandemic on 11$^{\text{th}}$ March, 2020 (*5*). In the UK, pandemic preparedness plans, developed since 2009 A/H1N1pdm, were rapidly activated with governmental emergency bodies and advisory groups convening before the end of January (*6*).

The UK Response to the COVID-19 pandemic escalated from an initial containment effort to the suppression or 'lock-down' strategy introduced on the 23$^{\text{rd}}$ of March (*7*). Over this period, through participation in governmental advisory groups, scientists from a number of research institutions fed into the pandemic decision-making processes. Quantitative understanding of the pandemic was based on the work of SPI-M (Scientific Pandemic Influenza Sub-Group on Modelling) (*8*). This work has informed the various phases of the UK response, from constructing planning scenarios for the health system, to monitoring these scenarios through regular nowcasting of new infections and forecasting of severe disease and health service demand, see (*9,10*) and papers available from (*8*).

Here we report the work of one of the participating groups, the Public Health England (PHE)/University of Cambridge modelling group. This collaboration, funded to develop modelling methodology for real-time pandemic influenza monitoring (*11*), was re-activated for the

COVID-19 pandemic (*12*). The age and spatially structured transmission model developed for influenza (*13, 14*), was re-purposed and, as data have increasingly become available, continuously adapted to SARS-COV-2 epidemiology, see Supplementary Materials (SM) 'Transmission Model'.

The model is implemented through a Bayesian statistical analysis of pandemic surveillance data, incorporating information on the natural history of infection from emerging literature. The surveillance data used are age- and region-specific counts of deaths of people with a lab-confirmed CoVID-19 diagnosis (see Fig. 1A-B); and, from 21^{st} April onwards, weekly batches of serological data, indicating the fraction of the population carrying CoVID-19 antibodies, from NHS Blood and Transplant (NHSBT) samples (see Fig. 1C) (*15*). The Wuhan outbreak additionally informs estimation of model parameters: the duration of infectiousness, the mean time from infection to symptom onset (*16*); and mean time from symptoms onset to death (*17*). Central to age-specific epidemic modelling, contact patterns between age groups have been derived from the POLYMOD study (*18*) stratified by setting (school, workplace, leisure etc), with these matrices sequentially updated using the Google mobility study and the UK time-use survey (*19*), to quantify the change in population mobility and access to these contact settings over time.

This transmission model has been used consistently throughout the pandemic. Through this regular monitoring we have been able to: anticipate and understand the impact of the lock-down; provide sequential updates of the pandemic dynamics, by estimating the basic (R_0) and effective (R_t) reproduction numbers, (*i.e.* the average number of individuals infected by an infectious individual in: a totally susceptible population with no control measures; and a partially susceptible population under some control measures respectively); and inform the gradual relaxation of the lock-down.

Here we focus on the contribution of our work at specific dates spanning three key periods:

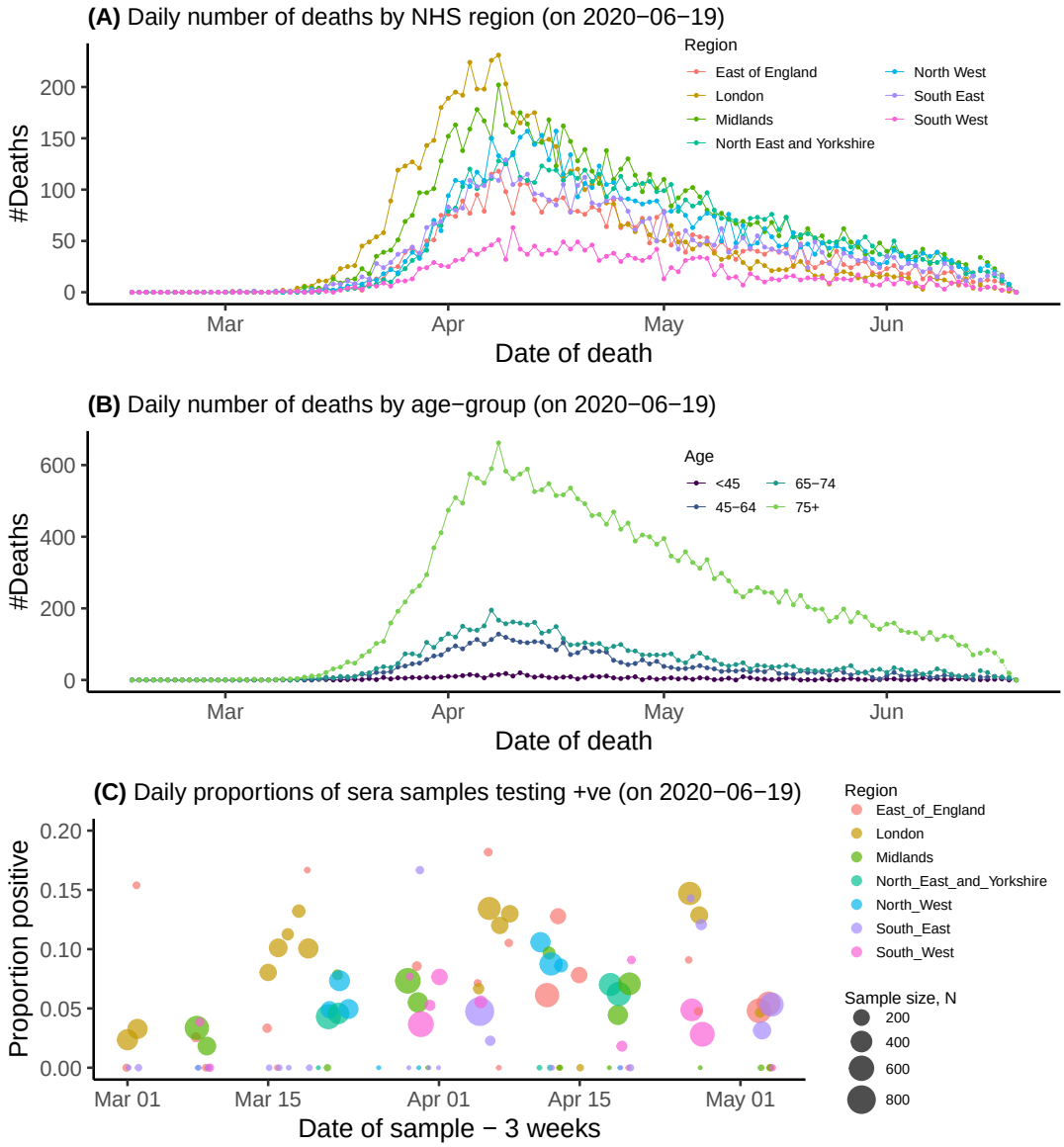

Figure 1: (A) Data on deaths by region, and (B) age; (C) Serological positivity by region and sampling date.

pre-lock-down (before 23rd of March), lock-down (until 11th May); and two subsequent dates that allow the assessment of the gradual easing of the lock-down.

Pre-lock-down After initial attempts to contain the pandemic through trace and test strategies (*20*) and to mitigate the burden on the National Health Service (NHS) through combinations of non-pharmaceutical interventions (*e.g.* case isolation, restrictions on foreign travel, shielding of vulnerable groups, cancellation of mass gatherings), the pressing question became: what level of stringent social distancing measures would be necessary to suppress transmission? At this stage, infection was not sufficiently widespread in each of the seven NHS regions for the data to inform a fully stratified model, by this time there had only been four deaths in the whole of the South-West. Therefore, no age structure was used and the country was stratified into two regions: London, where the number of deaths was significantly higher (Fig 1A), and Outside London. Assuming a pandemic intervention is imposed on 23^{rd} March, the model was fitted to data on CoVID-19 confirmed deaths to 15^{th} March, and then used to project epidemic curves forward a further eight weeks. These projections assumed differing reductions in contact rates (24%, 48%, 64%) (see Equation (6), SM) and consequently transmission.

Fig. 2 shows the projections for different levels of this reduction. The dashed red vertical line shows the date of the most recent data included in the analysis and the dashed purple line represents the timing of the intervention. Each column shows the projected epidemic infection and death rates under three assumed intervention impacts.

The most optimistic scenario in Fig. 2 corresponded to an immediate 64% reduction in transmission. Under this assumption, R_t was estimated to be 1.2 (95% CrI: 0.83–2.1) in London and 1.2 (95% CrI: 0.84–2.2) elsewhere. In this scenario, the probability that the imposed measures were successful in reducing R_t to the threshold of 1 required for declining transmission was only 19% and 17% in the two regions respectively. To be 95% certain that the intervention would lead to a sustained decline in infection, the intervention would need to induce an 81% reduction in transmission. Such a reduction could only be achieved through the implementation of extreme mitigation measures.

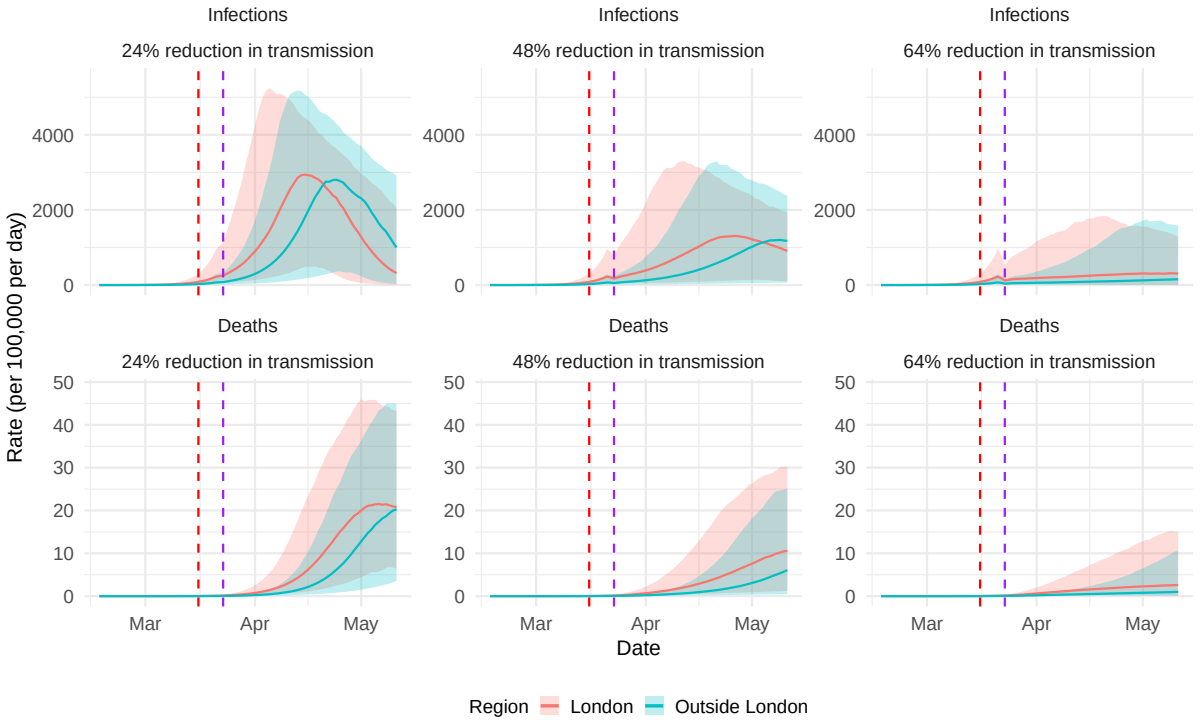

Figure 2: Estimated and projected COVID-19 infections and deaths by efficacy of social restriction measures.

The lock-down period The number of deaths continued to rise until April 8th, particularly in older age-groups (Fig. 1(B)), permitting stratification of the model by both age (8 groups) and region (7 NHS regions). Also new information from serological studies (Fig. 1(C)) started to become available and weekly data downloaded from the Google mobility survey could be used to update contact matrices.

A rhythm for pandemic monitoring was established. The model was run daily, with results feeding into local planning tools as well as the SPI-M consensus view on the state of the pandemic, and with periodic publication of web-reports summarising the latest results (*21*). These outputs included a number of key indicators: regional estimates of R_t and epidemic growth rates r, indicating whether transmission is increasing ($R_t > 1$) and the rate at which it is increasing (*22*); region and age-specific attack rates (*i.e.* the proportion of the population

already infected); and predictions of the burden due to mortality, both in terms of age-specific infection-fatality ratios and number of CoVID19 deaths. Public attention has focused on R_t as a headline figure for the state of the pandemic, but a more complete assessment requires all these indicators. Table 1 presents estimates of a selection of these indicators, giving snapshots of the pandemic state at the three chosen times.

The 10^{th} May section of the table shows the success of the lock-down at curtailing transmission: the R_t in England is now estimated to be 0.75 (95% CrI: 0.72–0.77) having dropped from 2.6 (95% CrI: 2.4–2.9) to 0.61 (95% CrI: 0.57–0.67) at the time of the lock-down, a reduction of 75% (95% CrI: 73%–77%), in line with the anticipation of the pre-lock-down modelling. The 'growth' rate for England indicates the daily number of infections were halving every $\log(2)/r$ = 11.5 days. London stands out as the region with the highest estimated attack rate (20% of people infected, CrI: 16%–26%), largely due to pre-lock-down levels of infection; the largest reduction in transmission, a drop of 81% (95% CrI: 77%–84%) to $R_t = 0.4$, 95% CrI: 0.36–0.43, and the steepest rates of decline in both the number of infections (halving every 4 days) and the observed fall in the number of deaths (Fig. 1A). The temporal patterns in infection are disrupted at the lock-down date, with the top row of Fig. 3(A) illustrating the size of this effect for both the London and North West Regions, alongside the estimated R_t.

Launched on the 10^{th} May, the UK COVID 4-level Alert System, co-ordinated by the newly established Joint Biosecurity Centre (JBC) and based on both estimated R_t and current infections, highlighted the key role of these indicators (*7*) in guiding the relaxation of lock-down measures without re-igniting transmission.

Lock-down Relaxation The first tranche of relaxations were announced on the 10^{th} May. From this time, accounting for likely changes in behaviour became crucial. In addition, it was clear, from the over-precision of the estimates of both incidence and R_t in the top row of

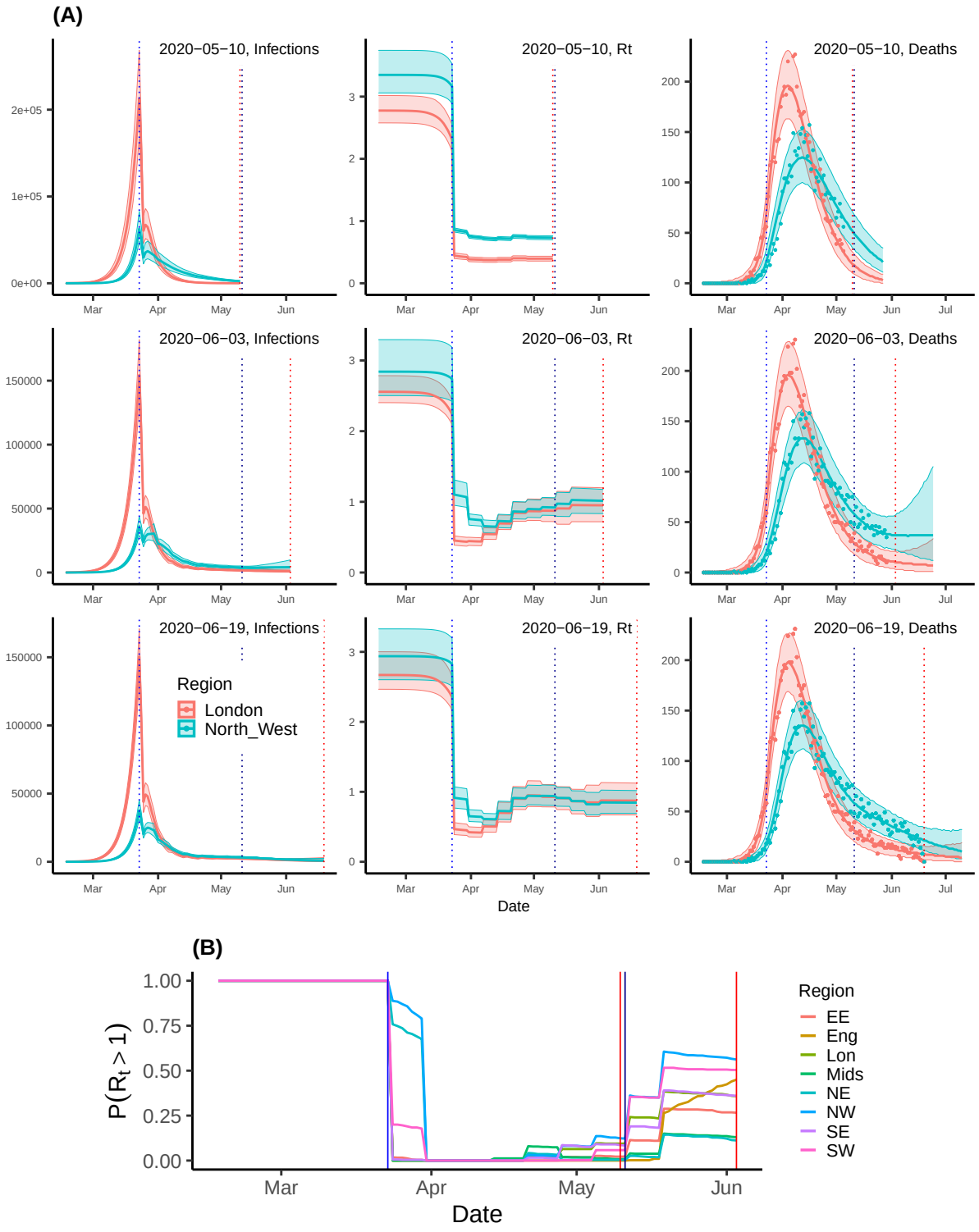

Figure 3: (A) Sequentially obtained estimates infection trajectories; R_t; and three week forecast of the number of deaths by date of analysis (rows). (B) Probability that R_t exceeds 1 as of 3rd June, by region. See SM, Fig. S1 for 10th May8and 19th June. In both plots, vertical blue lines indicate the timings of significant policy changes, vertical red lines indicate the time of analysis.

Table 1: Table of estimates (with 95% credible intervals attached) for key epidemic parameters and derived quantities.

Region	R_t	r	Infections	AR	IFR(overall)	IFR(75+)
			10th May			
East	0.71	-0.07	1,130	10%	-	-
	(0.68–0.74)	(-0.08– -0.06)	(758– 1,660)	(8%–13%)	-	-
London	0.40	-0.18	24	20%	-	-
	(0.36–0.43)	(-0.20– -0.16)	(10 – 53)	(16%–26%)	-	-
Mids	0.68	-0.08	1,490	11%	-	-
	(0.65–0.71)	(-0.08– -0.07)	(1,080– 2,040)	(9%–15%)	-	-
NE&Y	0.80	-0.05	4,320	11%	-	-
	(0.76–0.83)	(-0.05– -0.04)	(3,230– 5,650)	(8%–14%)	-	-
North West	0.73	-0.06	2,380	14%	-	-
	(0.70–0.76)	(-0.07– -0.06)	(1,750– 3,160)	(11%–18%)	-	-
South East	0.71	-0.07	1,260	8%	-	-
	(0.68–0.74)	(-0.08– -0.06)	(855– 1,810)	(6%–11%)	-	-
South West	0.76	-0.06	739	5%	-	-
	(0.72–0.80)	(-0.07– -0.05)	(438– 1,200)	(4%–6%)	-	-
England	0.75	-0.06	11,400	12%	0.6%	16%
	0.72–0.77	-0.06– -0.05	9,150-14,200	9%–15%	0.5%–0.8%	12%–21%
Region			**3rd June**			
East	0.94	-0.01	1,660	9%	-	-
	(0.73–1.14)	(-0.06–0.03)	(502– 4,610)	(8%–10%)	-	-
London	0.95	-0.01	1,310	17%	-	-
	(0.72–1.20)	(-0.07–0.04)	(247 – 4,670)	(15% – 19%)	-	-
Mids	0.90	-0.02	2,460	10%	-	-
	(0.73–1.07)	(-0.07–0.01)	(809– 6,070)	(9%–11%)	-	-
NE&Y	0.89	-0.02	2,450	9%	-	-
	(0.75–1.04)	(-0.07–0.01)	(865– 5,870)	(8%–11%)	-	-
North West	1.01	0.0	4,170	12%	-	-
	(0.83–1.18)	0.0 (-0.04–0.04)	(1,580– 9,840)	(10%–14%)	-	-
South East	0.97	-0.01	2,420	7%	-	-
	(0.78–1.17)	(-0.05– -0.03)	(782– 6,040)	(6%–8%)	-	-
South West	1.00	0.0	778	4%	-	-
	(0.77–1.29)	(-0.06–0.06)	(162– 3,080)	(3%–5%)	-	-
England	0.99	0.0	16,700	10%	0.9%	23%
	0.91–1.09	-0.02–0.02	10,700–25,300	9%–11%	0.8%–1.0%	20%–27%
Region			**19th June**			
East	0.80	-0.05	292	7%	-	-
	0.60–1.01	-0.10–0.00	60–1,050	6%–8%	-	-
London	0.87	-0.03	837	17%	-	-
	0.67–1.12	-0.08–0.02	159–3,070	15%–18%	-	-
Mids	0.82	-0.04	709	8%	-	-
	0.64–1.01	-0.09–0.00	189–2,040	7%–9%	-	-
NE&Y	0.76	-0.05	351	7%	-	-
	0.58–0.95	-0.11– -0.01	84–1,110	6%–8%	-	-
North West	0.84	-0.04	872	10%	-	-
	0.69–1.02	-0.08–0.00	255–2,460	9%–11%	-	-
South East	0.77	-0.05	342	6%	-	-
	0.59–0.96	-0.10– -0.01	79–1,120	5%–6%	-	-
South West	0.94	-0.01	312	3%	-	-
	0.69–1.21	-0.07–0.04	60–1,180	3%–4%	-	-
England	0.88	-0.03	4,260	8%	1.1%	17%
	0.79–1.01	-0.05–0.00	2,370–7,290	8%–9%	0.9–1.4%	14%–22%

Fig. 3(A), that the model required a greater flexibility to capture such changing behaviours. From an appropriately adapted model (see SM 'Transmission model' for details), we estimated

that at the 3rd June, R_t for England reached 0.99 (95% CrI: 0.91–1.09), with the probability of exceeding the value of 1 rapidly increasing over time (see Fig. 3(B)). This figure masks regional heterogeneity in transmission. The North West and the South West were characterised by R_t values above 1 (with a probability $R_t > 1$ of over 50%, Fig. 3(B)) and growth rate estimates encompassing positive values. For the North West, we estimated 4,170 (95% CrI:1,580–9,840) daily infections, the highest number in the country (see Table 1). The step changes in the plots of R_t over time in Fig. 3 for 10th May are entirely due to changes in the Google mobility matrices. Looking at the equivalent plot for the 3rd June analysis, over the same interval, the step changes are larger. This difference in the level of fluctuation over time suggests that the increases in R_t are too large to be solely attributed to mobility-driven changes in the contact matrices. Furthermore, for the North West, the drop in R_t around the lock-down is not as sharp as in London, but rather staggered over three weeks. This might suggest a different response to the lock-down in these two regions, which we had previously not been able to identify. The estimated steady resurgence of R_t in the North West ultimately led to a policy change, delaying the staged re-opening of schools (*23*).

Continuing to monitor the pandemic evolution in the post-lock-down era, we adapted the model to incorporate new evidence on differential susceptibility to infection by age (*24*) (see SM, around equation (7)). Results from 19th June data (Table 1, Fig. 3(A)) show lower estimates for R_t, negative growth rates and the estimated number of infections in England decreasing to 4,300 (95% CrI: 2,400 – 7,300). There is still regional heterogeneity, with two regions for which the credible intervals for R_t exclude 1 (North East & Yorkshire, and the South East); and the probability that the epidemic is growing is 30% in the South West and below 15% in each of the other regions (Fig S1(B), SM). Throughout we have been estimating age-specific infection-fatality ratios (see Tables 1 and S4). Allowing for differential age susceptibility, the age-specific estimates of the infection-fatality ratio fall to 17% (95% CrI: 14%–22%) in the over-75s (from

23%, 95% CrI: 20%–27%) with a rise to 2.9% in the 65–74ys, (see Table S4) and to 1.1% (95% CrI: 0.9%–1.4%) from 0.9% (95% CrI: 0.8%–1.0%) overall. These less severe estimates (in comparison to the 3rd June analysis) led to the UK Chief Medical Officers agreeing with a JBC recommendation that the alert level should be downgraded to level three.

Discussion Since the 19th of June, weekly updates have continued to be posted online (*21*). Recent estimates of the IFR have varied in the region of 0.9% to 1.4% overall and 14% to 19% in the over-75s. R_t is approaching the value of 1 in most regions without exceeding it, which, together with a decreasing number of daily infections indicates an epidemic still in decline, although local outbreaks are being increasingly detected (*25*). The estimates presented here are consistent with the SPI-M consensus on the values of R_t both nationally and regionally (*26*). Incidence estimates can be contrasted with estimates from community cross-sectional studies. In a report of the 9th July, the Office for National Statistics (ONS) estimates 1,700 (range 700–3,700) new daily infections over the two weeks leading up to 4th July (*27*), while the ZOE study (*28*) reports an average 1,470 infections per day over a similar period. In our work incidence ranges from a central estimate of 4,200 daily infections down to 3,500 over the period. These are not incongruous to the ZOE app estimates, which only records symptomatic infection and require some scaling to derive an estimate for total infections. The ONS estimate is likely to be an under-estimate as the survey does not include individuals in institutionalised settings *e.g.* care homes, where incidence may be far higher than in the community. The degree to which this is an under-estimate, however, is unclear.

The ONS also reports (*29*) that 6.3% (95% CrI: 4.7%–8.1%) of individuals showed the presence of antibodies to the COVID-19 in blood sera samples (as of 19th June), a little lower than the 8% estimated attack rate for England. This discrepancy may well be due to the timing of the samples, due to the waning of the antibody response over time. Estimates of attack rates

(see Table 1) show that our belief on the proportion of the population that has been infected is being revised downwards at each sequential analysis. This, together with the emerging evidence of waning immunity (*30*), paint a muddied picture in term of potential for a population-level resurgence in infection.

On the 4^{th} July there was a significant step change in the gradual relaxation of pandemic mitigation measures as leisure facilities, tourist attractions, pubs and cafes all became accessible to the public once again (*31*). The impact of this is still largely to be observed and assessed. If the concerning worse-case scenario presented for the Winter in the recent publication of the Academy of Medical Science (*32*) comes through, we will be facing a very challenging second wave. Our monitoring tool, continuously adapted to incorporate the accumulating surveillance data, will be key to providing quantification of all aspects of any resurgence.

Acknowledgements

This work was supported by the Medical Research Council (Unit programme number MC UU 00002/11) in partnership with Public Health England. Prior to the pandemic, the project was developed under a grant from the National Institute for Health Research (HTA Project: 11/46/03). We gratefully acknowledge the access to the data from the United Kingdom Time Use Survey through the UK Data Service (`http://doi.org/10.5255/UKDA-SN-8128-1`). We acknowledge the support of the PHE Epidemiology Cell in consistently providing the data streams used. We would also like to thank Dr Nigel Gay for the initial development of the model and constructive comments on the manuscript. This work has also benefited from insightful discussions with Dr Petra Klepac.

The core membership of the PHE Modelling Cell consists of: Abbygail Jaccard, Andre Charlett, Anna Rance, Anne Presanis, Archana Purohit, Brian Ferguson, Brodie Walker, David Mustard, Declan Bays, Dianne Addei, Emilia Vynnycky, Emily Agnew, Emma Bennett, Emma

Gillingham, Hannah Williams, Ian Hall, James Lewis, Jonathan Carruthers, Joseph Shingleton, Joshua Blake, Judith Field, Martin Grunnill, Matt Edmunds, Matt Hennessey, Nick Gent, Peter White, Simona Baracaia, Stephanie Shadwell, Steven Dyke, Thomas Finnie, Virginia Cox and Xu-Sheng Zhang.

References

1. World Health Organization, Pneumonia of unknown cause - China, https://www.who.int/csr/don/05-january-2020-pneumonia-of-unkown-cause-china/en/ (2020). WHO, Accessed 25 June, 2020.

2. Center for Systems Science and Engineering (CSSE), Johns Hopkins University, COVID-19 Case Tracker, https://coronavirus.jhu.edu/map.html (2020). Johns Hopkins University, Accessed 25 June, 2020.

3. J. M. Read, J. R. Bridgen, D. A. Cummings, A. Ho, C. P. Jewell, *medRxiv* p. 2020.01.23.20018549 (2020).

4. G. Spiteri, *et al.*, *Eurosurveillance* **25**, 2000178 (2020).

5. World Health Organization, WHO Director-General's opening remarks at the media briefing on COVID-19 – 11 March 2020, https://www.who.int/dg/speeches/detail/who-director-general-s-opening-remarks-at-the-media-briefing-on-covid-19---11-march-2020 (2020). WHO, Accessed 25 June, 2020.

6. UK Government, Precautionary SAGE meeting on Wuhan Coronavirus (WN-CoV), https://assets.publishing.service.gov.uk/government/uploads/system/uploads/attachment_data/file/888767/S0369_

Precautionary_SAGE_meeting_on_Wuhan_Coronavirus__WN-CoV__.pdf (2020). UK Government, Accessed 9 July, 2020.

7. UK Government, Prime Minister's statment on coronavirus (COVID-19): 23 March 2020, https://www.gov.uk/government/speeches/pm-address-to-the-nation-on-coronavirus-23-march-2020 (2020). UK Government, Accessed 9 July, 2020.

8. UK Government, Scientific Advisory Group for Emergences (SAGE): Coronavirus (COVID-19) response, https://www.gov.uk/government/groups/scientific-advisory-group-for-emergencies-sage-coronavirus-covid-19-response (2020). UK Government, Accessed 9 July, 2020.

9. S. Abbott, *et al.*, *Wellcome Open Research* **5**, 112 (2020).

10. M. J. Keeling, *et al.*, *medRxiv* p. 2020.05.10.20083683 (2020).

11. C. Simpson, D. Beever, K. Challen, E. Al., *Lancet Infect Dis* **19**, 295 (2019).

12. C. R. Simpson, *et al.*, The UK hibernated pandemic influenza research portfolio: triggered for COVID-19 (2020).

13. P. J. Birrell, X.-S. Zhang, R. G. Pebody, N. J. Gay, D. De Angelis, *Scientific Reports* **6**, 29004 (2016).

14. P. Birrell, R. Pebody, A. Charlett, X.-S. Zhang, D. De Angelis, *Health Technology Assessment* **21** (2017).

15. Public Health England Surveillance Cell, Serological Surveillance: Summary Report 3, https://assets.publishing.service.gov.uk/government/

uploads/system/uploads/attachment_data/file/890194/s0337-serological-surveillance-summary-3-060520-sage34.pdf (2020). PHE, Accessed 12 July, 2020.

16. Q. Li, *et al.*, *New England Journal of Medicine* **382**, 1199 (2020).

17. R. Verity, *et al.*, *The Lancet Infectious Diseases* (2020).

18. J. Mossong, *et al.*, *PLoS Medicine* **5**, 0381 (2008).

19. E. van Leeuwen, {PHE Joint modelling cell}, F. Sandmann, *medRxiv* p. 2020.06.03.20067793 (2020).

20. N. L. Boddington, *et al.*, *medRxiv* p. 2020.05.18.20086157 (2020).

21. P. J. Birrell, J. Blake, E. van Leeuwen, D. De Angelis, Nowcasting and forecasting of COVID-19, https://www.mrc-bsu.cam.ac.uk/tackling-covid-19/nowcasting-and-forecasting-of-covid-19/ (2020). MRC-BSU, Accessed 13 July, 2020.

22. Gog, Julia and Thomas, Rachel and Freiberger, Marianne, The growth rate of COVID-19, https://plus.maths.org/content/epidemic-growth-rate (2020). +plus magazine, Accessed 14 July, 2020.

23. The Guardian, https://www.theguardian.com/education/2020/jun/06/schools-north-west-england-postpone-reopening-coronavirus (2020). The Guardian, Accessed 14 July, 2020.

24. R. M. Viner, *et al.*, *medRxiv* p. 2020.05.20.20108126 (2020).

25. E. Mahase, *BMJ (Clinical research ed.)* **369**, m2635 (2020).

26. UK Government, The R number and growth rate in the UK, https://www.gov.uk/guidance/the-r-number-in-the-uk (2020). UK Government, Accessed 14 July, 2020.

27. Office for National Statistics: COVID-19 Infection Survey, https://www.ons.gov.uk/peoplepopulationandcommunity/healthandsocialcare/conditionsanddiseases/bulletins/coronaviruscovid19infectionsurveypilot/england9july2020#incidence-rate (2020). Office for National Statistics.

28. COVID Symptom Study, https://covid.joinzoe.com/post/covid-incidence-uk (2020). COVID Symptom Study, Accessed 13 July, 2020.

29. Office for National Statistics: COVID-19 Infection Survey, https://www.ons.gov.uk/peoplepopulationandcommunity/healthandsocialcare/conditionsanddiseases/bulletins/coronaviruscovid19infectionsurveypilot/2july2020#antibody-data (2020). Office for National Statistics.

30. J. Seow, *et al.*, *medRxiv* p. 2020.07.09.20148429 (2020).

31. Dunn, Phoebe and Allen, Lucinda and Cameron, Genevieve and Alderwick, Hugh, COVID-19 policy tracker, https://www.health.org.uk/news-and-comment/charts-and-infographics/covid-19-policy-tracker (2020). The Health Foundation, Accessed 13 July, 2020.

32. The Academy of Medical Sciences, https://acmedsci.ac.uk/file-download/51353957 (2020). The Academy of Medical Sciences, Accessed 14 July, 2020.

33. UK Government, Coronavirus (COVID-19) in the UK, https://coronavirus.data.gov.uk/ (2020). UK Government, Accessed 12 June, 2020.

34. UK Government, Number of coronavirus (COVID-19) cases and risk in the UK, https://www.gov.uk/guidance/coronavirus-covid-19-information-for-the-public (2020). UK Government, Accessed 12 June, 2020.

35. J. Duggan, Rare and Imported Pathogens Laboratory, Public Health England, Evaluation of the Euroimmun Anti-SARS-CoV-2 ELISA (IgG) serology assay for the detection of anti-SARS-CoV-2 antibodies, https://assets.publishing.service.gov.uk/government/uploads/system/uploads/attachment_data/file/893433/Evaluation_of_Euroimmun_SARS_CoV_2_ELISA_IgG__1_.pdf (2020). Public Health England, Accessed 20 July, 2020.

36. S. Funk, socialmixr: Social mixing matrices for infectious disease modelling, The Comprehensive R Archive Network, http://datacompass.lshtm.ac.uk/646/ (2018).

Supplementary Materials - Real-time Nowcasting and Forecasting of COVID-19 Dynamics in England: the first wave?

Methods

Surveillance data

The UK confirmed its first case of CoVID infection, imported from China, on the 30^{th} January, with the first CoVID-linked death reported on the 6^{th} March. Initially deaths were monitored by date of report, (*33*) with a full line-listing of deaths being made available by PHE from the 21^{st} March, enabling tracking of the pandemic using actual dates of death.

Prior to this time, the most complete data were the time series of reported cases, individuals who have a returned a PCR-positive swab sample. (*33*) Initial analyses of the pandemic were based on either or both of these datasets, attempting to quantify the emerging pandemic but also to monitor the degree of coherence between the datasets. However, rates of testing and the country's testing capacity were significantly increasing, (*34*), whilst government policy was changing the testing threshold. These led to a significant ascertainment bias to the confirmed case data which in turn would lead to estimated incidence curves based on these data to be significantly skewed.

A third data source was the testing of residual blood sera from blood donors in England via National Health Service Blood and Transplant (NHSBT). These data inform the population prevalence of antibodies, informing the fraction of the population that have ever been infected. From repeated follow-up of known infections, 74.7% (*35*) of infections return a positive result for the presence of antibodies within 21 days of the onset of symptoms

Transmission Model

An age stratified transmission model is fitted to each region under study simultaneously with the sharing of some global parameters. Within each region, the transmission dynamics are governed

by a system of ordinary differential equations, discretised to give the following set of first order difference equations:

$$\begin{aligned}
S_{r,t_k,i} &= S_{r,t_{k-1},i}\left(1-\lambda_{r,t_{k-1},i}\delta t\right)\\
E^1_{r,t_k,i} &= E^1_{r,t_{k-1},i}\left(1-\frac{2\delta t}{d_L}\right)+S_{r,t_{k-1},i}\lambda_{r,t_{k-1},i}\delta t\\
E^2_{r,t_k,i} &= E^2_{r,t_{k-1},i}\left(1-\frac{2\delta t}{d_L}\right)+E^1_{r,t_{k-1},i}\frac{2\delta t}{d_L}\\
I^1_{r,t_k,i} &= I^1_{r,t_{k-1},i}\left(1-\frac{2\delta t}{d_I}\right)+E^2_{r,t_{k-1},i}\frac{2\delta t}{d_L}\\
I^2_{r,t_k,i} &= I^2_{r,t_{k-1},i}\left(1-\frac{2\delta t}{d_I}\right)+I^1_{r,t_{k-1},i}\frac{2\delta t}{d_I}
\end{aligned} \tag{1}$$

where: $S_{r,t_k,i}$, $E^d_{r,t_k,i}$, $I^d_{r,t_k,i}, d=1,2$ represent the time $t_k, k=1,\ldots,K$, partitioning of the population of individuals in a region $r, r=1,\ldots,n_r$, in age-group $i, i=1,\ldots,n_A$, into S (susceptible), E (exposed) and I (infectious) disease states. The mean latent and infectious periods are d_L and d_I respectively; and $\lambda_{r,t_k,i}$ is the time- and age-varying rate with which susceptible individuals become infected. Time steps of $\delta t = 0.5$ days are chosen to be sufficiently small relative to the anticipated latent and infectious periods. New infections are generated as

$$\Delta^{\text{infec}}_{r,t_k,i} = S_{r,t_k,i}p^{\lambda}_{r,t_k,i}, \tag{2}$$

where

$$p^{\lambda}_{r,t_k,i} = \left(1-\prod_{j=1}^{n_A}\left[\left(1-b^{t_k}_{r,ij}\right)^{I^1_{r,t_k,j}+I^2_{r,t_k,j}}\right]\right)\delta t \approx \lambda_{r,t_k,i}\delta t. \tag{3}$$

Here, $b^{t_k}_{r,ij}$ is the probability of a susceptible individual in region r of age group i being infected by an infectious individual in age group j at time t_k. It is a function of:

- a set of time-varying contact matrices $\boldsymbol{C}^{t_k} = \left\{C^{t_k}_{ij}\right\}$, the entries of which describe the expected number of contacts between any two individuals of the different strata within a single time unit.

- $\boldsymbol{M}_r^{t_k} = \left\{M_{r,ij}^{t_k}\right\}$, a region-specific matrix, the $(i,j)^{\text{th}}$ element of which gives the relative susceptibility of someone in age-group i to an infection from an infectious individual in age-group j assuming contact between the two.

- $\beta_{t_k,r}$, a time-varying parameter encapsulating further temporal fluctuation in transmission that applies to all ages.

- $R_{0,r}$ are the initial reproduction numbers for the pandemic in each region at time t_0

- $R_{0,r}^*$ are the dominant eigenvalues of the initial next-generation matrices, $\Lambda_{0,r}$ such that

$$\Lambda_{0,r,ij} = N_{r,i}\tilde{C}_{r,ij}^{t_0} d_I, \tag{4}$$

  where $N_{r,i}$ is the population size in region r and age-group i, and $\tilde{C}_r^{t_k}$ are a set of matrices defined by

$$\tilde{\boldsymbol{C}}_r^{t_k} = \boldsymbol{C}^{t_k} \odot \boldsymbol{M}_r^{t_k}$$

  where the $\odot$ notation indicates element-wise multiplication, s.t $A = B \odot C$ if $A_{ij} = B_{ij}C_{ij}$.

As described in the following sub-section, the $\boldsymbol{C}^{t_k}$ matrices encode the information contained about contact rates between different age groups derived from the POLYMOD study (*18*), Google mobility and the time-use survey. The $\boldsymbol{M}_r^{t_k}$ matrices capture any mis-specification of these matrices in terms of the changing pattern of infection between the age groups, whereas the β_{t_k} parameters account for mis-specification of the changing scale of transmission over time as described by the matrices.

In the main manuscript, a number of model developments are identified that were implemented in between the analyses presented. The general expression of $b_{r,ij}^{t_k}$ is:

$$b_{r,ij}^{t_k} = \frac{\beta_{t_k,r} R_{0,r}}{R_{0,r}^*} \tilde{C}_{r,ij}^{t_k}; \tag{5}$$

but each of the models implemented constitute some simplification of this expression. These model developments are itemised here, starting with the earliest, and most simple, analysis:

- **20th March**: No age dimension to the analysis, so transmission was simply broken up with a changepoint at $t_k = t_{\text{lock}}$. The dynamics of the two regions (London, Outside London) differed only in that they had a differing initial seeding of infection. Here $M_{r,ij}^{t_k} = (1 - \mathbb{1}_{t_k \geq t_{\text{lock}}}(1-m))$ and $C_{ij}^{t_k} = 1$, giving m the interpretation as a global change in the susceptibility to infection given contact with an infectious individual. From (4), $R_{0,r}^{*} = N_r d_I$. Simplifying (5):

$$b_{r,ij}^{t_k} = (1 - \mathbb{1}_{t_k \geq t_{\text{lock}}}(1-m))\frac{R_{0,r}}{N_r d_I}. \tag{6}$$

- **10th May**: Analysis is now age-specific. Reproduction number $R_{0,r}$ and susceptibility parameter m_r now region-specific. The matrices $\boldsymbol{M}_r^{t_k}$ are a matrix extension of the 20th March analysis:

$$\boldsymbol{M}_r^{t_k} = (1 - \mathbb{1}_{t_k \geq t_{\text{lock}}}(1-m_r))\,\mathbf{1}_{n_A}\mathbf{1}_{n_A}^T,$$

where the susceptibility parameter m_r now has region dependence, $\mathbf{1}_{n_A}$ is a vector of ones of length n_A, and $\mathbf{1}_{n_A}\mathbf{1}_{n_A}^T$ is a corresponding matrix of ones. This has no age dependence, and so it is assumed that the POLYMOD and Google-derived matrices, $\boldsymbol{C}_r^{t_k}$, accurately account for changing patterns of infection over time). Again (4) can be simplified to:

$$b_{r,ij}^{t_k} = (1 - \mathbb{1}_{t_k \geq t_{\text{lock}}}(1-m_r))\frac{R_{0,r}}{R_{0,r}^{*}}C_{ij}^{t_k}$$

- **3rd June**: Introduction of the time-varying transmissibility parameter, $\beta_{t_k,r}$. It was decided to change these piecewise with weekly changepoints. Denote $w_k \equiv w(t_k)$ giving the week in which time t_k falls. Over time these are not allowed to vary unconstrained and

a smoothing is imposed by assuming, *a priori* that they develop according to a random-walk.

$$\log\left(\beta_{w_k,r}\right) \sim \mathrm{N}\left(\log\left(\beta_{w_{k-1},r}\right), \sigma_\beta^2\right), \quad \beta_{w_{\text{lock}},r} = 1.$$

Where $\beta_{w_{\text{lock}},r}$ is the rate that applies in all weeks up to and including the first week of the lock-down. As all other components of the model remain unchanged, the form for $b_{r,ij}^{t_k}$ is:

$$b_{r,ij}^{t_k} = \left(1 - \mathbb{1}_{t_k \geq t_{\text{lock}}}\left(1 - m_r\right)\right) \frac{\beta_{w_k,r} R_{0,r}}{R_{0,r}^*} C_{ij}^{t_k}.$$

- **19th June**: Separate levels of susceptibility are introduced for the over-75s, both before and after the lock-down to account for some lack of fit. To characterise this, we need to define two matrices, $\boldsymbol{M}_r^{t_{\text{lock}}-}$ and $\boldsymbol{M}_r^{t_{\text{lock}}+}$ that apply before and after t_{lock} respectively,

$$M_{r,ij}^{t_{\text{lock}}-} = \begin{cases} m_{r,1} & i = \{\geq 75\} \\ 1 & \text{otherwise} \end{cases}; \qquad M_{r,ij}^{t_{\text{lock}}+} = \begin{cases} m_{r,3} & i = \{\geq 75\} \\ m_{r,2} & \text{otherwise} \end{cases},$$

such that

$$\tilde{\boldsymbol{C}}_r^{t_k} = \begin{cases} \boldsymbol{M}_r^{t_{\text{lock}}-} \odot \boldsymbol{C}^{t_k} & t_k < t_{\text{lock}} \\ \boldsymbol{M}_r^{t_{\text{lock}}+} \odot \boldsymbol{C}^{t_k} & t_k \geq t_{\text{lock}} \end{cases}.$$

We would then feed back into equation (3):

$$b_{r,ij}^{t_k} = \frac{\beta_{w_k,r} R_{0,r}}{R_{0,r}^*} \tilde{C}_{r,ij}^{t_k}. \tag{7}$$

Calculating $\mathbf{R}_t$ We estimate a region-specific parameter describing the initial exponential growth in infections, denoted ψ_r. Using the formula of Wearing et al. (2005), this is related to the initial reproduction number $R_{0,r}$ via the formula

$$R_{0,r} = \psi_r d_I \frac{\left(\frac{\psi_r d_L}{2} + 1\right)^2}{1 - \frac{1}{\left(\frac{\psi_r d_I}{2} + 1\right)^2}}.$$

Over time the value of the reproduction number will change as contact patterns shift and the supply of susceptible individuals deplete. The formula for the time-t reproduction number is

$$R_{t_k,r} = \begin{cases} R_{0,r}\frac{R^*_{t_k,r}}{R^*_{0,r}} & \text{if } t_k < t_{\text{lock}} \\ \beta_{w_k,r} R_{0,r}\frac{R^*_{t_k,r}}{R^*_{0,r}} & \text{if } t_k \geq t_{\text{lock}} \end{cases}$$

where $R^*_{t_k,r}$ is the dominant eigenvalue of the time t_k next-generation matrix, $\Lambda_{k,r}$, with elements:

$$(\Lambda_{k,r})_{ij} = S_{r,t_k,i}\tilde{C}^{t_k}_{r,ij} d_I$$

To get an 'all England' value for $R_{t_k,E}$ a weighted average of the regional $R_{t_k,r}$ is calculated, where the weights are given by the sum of the infections in each region:

$$R_{t_k,E} = \frac{\sum_r R_{t_k,r} \sum_i \Delta^{\text{infec}}_{r,t_k,i}}{\sum_r \sum_i \Delta^{\text{infec}}_{r,t_k,i}}$$

Contact matrices

Time dependent contact matrices are based on location-specific POLYMOD matrices (where locations include "at work", "at home", "on transport" etc), combined with the time-use survey (*19*) to identify 18 different activities, including school, work, social visits, shopping etc.. The traditional POLYMOD matrices are used until 23rd March, the time of the lockdown (*18, 36*). From this point on, the Google mobility and time-use survey data were used to calculate proportionate reductions in the location-specific POLYMOD matrices, which are summed together to give a weekly-varying contact matrix, $\boldsymbol{C}^{t_k} = \boldsymbol{C}^{w(t_k)} \equiv \boldsymbol{C}^{w_k}$.

Following (*19*) we identified 18 different activities (Table S1). Some of these activities were not allowed during lock down and, therefore, assumed to have been stopped. For other activities we used the most relevant data source. For some activities no suitable data source was available. In that case we used the retail and recreation mobility data provided by Google, because this data was assumed to best represent the general adherence level in the UK. For example, visits are unlikely to have stopped completely. Instead the retail and recreation level is used (Table

Table S1: The data sources used for the different activities identified by the time use survey. Values represent the assumed activity level. Where direct data was available we used other (live) data sources. Here GM represents the relevant Google mobility category.

activity	Data source
alone	1
bars and restaurants	0
bed	1
cultural	0
exercise indoors	0
home	1
library	0
school	Attendance records
visit	GM Retail & recreation
parks	GM Parks
holiday	GM Retail & recreation
shopping	GM Retail & recreation
exercise outdoors	GM Retail & recreation
exercise unspecified	GM Retail & recreation
shopping essential	GM Grocery & pharmacy
unspecified	GM Retail & recreation
work	GM Workplace
transport	GM Transit stations

Table S2: The fraction of contacts at home attributed to members of the household.

AgeGroup	Contacts at home	Max contacts with household members	fraction
$[0, 1)$	5.643	2.857	0.506
$[1, 5)$	4.295	2.808	0.654
$[5, 15)$	4.980	2.970	0.596
$[15, 25)$	4.206	2.675	0.636
$[25, 45)$	4.125	2.388	0.579
$[45, 65)$	3.767	1.524	0.405
$[65, 75)$	3.614	1.045	0.289
$[75, +)$	3.571	0.714	0.200

S1). Note that the activities which in a well mixed model have the most effect on the base reproductive number are school, work, visits and unspecified (*19*).

School attendance School size and age range is publicly available for England. We used this to calculate the number of students for each school in the modelled age groups, based on the assumption that the students were evenly distributed across different school years. We also had access to attendance levels over time for some schools. This data was then used to calculate the average weekly attendance level in each local authority, weighted by the size of the school in that age group. Finally, we combined these values to calculate attendance in England, weighted by local authority population size. Not all schools reported attendance every week, as a result the attendance by local authority was, in rare cases, only based on the report of 1 or more small schools. To ensure that these did not skew our results, we ignored any attendance estimate based on schools with less than 100 students in total.

Visits at home (*19*) used the time usage data for visits at home to estimate the number of visit related contacts at home. We found that this underestimates the number of visitors and instead used the POLYMOD data on household size to estimate the fraction of contacts at home with

other household members versus the contacts with others (e.g. visitors). First, we extracted the mean number of contacts at home (Table S2). Next, we limited numbers of contacts at home (c_i) to household size (h_i) minus one ($\hat{c_i} = \min(h_i - 1, c_i)$), i.e. the maximum number of contacts any participant (i) can have with just household members and calculated the mean contacts based on that value. Note that this provides a conservative estimate of the fraction of contacts from visits, because some participants will not have met all their household members during the day.

Google mobility data During the pandemic Google provided aggregated mobility data from Android phones for many countries (https://www.google.com/covid19/mobility/). The mobility data gives an indication of the activity level for 5 different activities: retail and recreation, grocery and pharmacy, parks, transit stations, workplaces and residential. The UK data was further subdivided into activity by local authority, by matching the Google provided locations to local authority districts in England. This data was then combined, weighted by population size. Finally, the daily values were averaged by week, to produce weekly activity levels.

Likelihood

Counts of deaths are assumed to have a negative binomial distribution. If $X_{r,t_k,i}$ is the number of observed deaths on day t_k in age group i in region r, then the expected number of deaths are derived using (2), an assumed-known distribution of the time from infection to death from COVID-19, f and an estimated age-specific infection-fatality ratio p_i:

$$\mu_{r,t_k,i} = p_i \sum_{l=0}^{k} f_{k-l} \Delta^{\text{infec}}_{r,t_l,i}$$

where f_l gives the probability the death occurs on the l^{th} day after infection. Then we assume

$$X_{r,t_k,i} \sim \text{NegBin}\left(\mu_{r,t_k,i}, \eta\right),$$

where η is a dispersion parameter such that $\mathbb{E}X_{r,t_k,i} = \mu_{r,t_k,i}$ and Var $(X_{r,t_k,i}) = \mu_{r,t_k,i}\,(1+\eta)$.

The serological data is dependent on two parameters, the sensitivity and the specificity of the serological testing process, k_{sens} and k_{spec} respectively. If, on day t_k, $n_{r,t_k,i}$ blood samples are taken from individuals in region r and age-group i, and the observed number of positive tests is $Y_{r,t_k,i}$, then

$$Y_{r,t_k,i} \sim Bin\left(n_{r,t_k,i}, k_{\text{sens}}\left(1 - \frac{S_{r,t_k,i}}{N_{r,i}}\right) + (1 - k_{\text{spec}})\,\frac{S_{r,t_k,i}}{N_{r,i}}\right).$$

Inference Table S3 contains a full list of parameters. The top portion refers to the unknown parameters that are estimated and the bottom portion contain parameters that have been fixed. Wherever possible, a brief justification of the chosen prior/value is given.

Table S3: Model parameters with assumed prior distributions or fixed values

Name	Prior source
Over-dispersion, η	Uninformative $\Gamma(1, 0.2)$
Mean infectious period, d_I	2 + $\Gamma(1.43, 0.549)$, based on Li et al (2020).
All contact matrix multipliers, $m_{r,l}, l = 1, \ldots, 3$	Uninformative $\Gamma(4, 4)$
Exponential growth, ψ_r	$\Gamma(31.36, 224)$, through matching to an uninformative R_0 given sampled values of d_I and assumed value of d_L.
Initial infection, I_0	Uninformative. To be described.
Infection-fatality rate p_i	Based on Verity et al. (2020).
Serological test sensitivity, k_{sens}	Based on convalescent sera, $\beta(71.5, 29.5)$.
Serological test specificity, k_{spec}	Based on pre-COVID sera, $\beta(777.5, 9.5)$.
Step-size on log-scale of weekly variation in transmission, σ_β	Informative $\Gamma(1, 100)$.
Mean latent period, d_L	4 days.
Mean (s.d) incubation period	4.0 (1.41) days.
Mean (s.d) time to death from symptom onset	15.0 (12.1) days.

Estimation is conducted in a Bayesian framework by combining the prior information and likelihoods specified above, to derive posterior distributions for the unknown parameters and

any functions of such parameters. Sampling from these posterior distribution is carried out through Markov chain Monte Carlo (*13, 14*). The most recent analysis featured in this paper was based on 900,000 iterations, with an initial adaptive phase of 45,000 iterations within a burn-in period of 90,000 iterations. Parameter estimates are based on the full sample following burn-in thinned to retain every 125 iterations, and projections are based on a sample thinned to every 250 iterations. All central estimates are pointwise medians of quantities calculated on the basis of this sample, and uncertainty is expressed through 95% credible intervals (CrI) derived from the 2.5% and 97.5% quantiles.

Additional Results

In Fig. S1, we present the region-specific probabilities that $R_t > 1$. In the 10^{th} May analysis, the plot is binary - R_t is definitely above the threshold before the lockdown, and we estimated the reduction in transmission to be sufficient to reduce it to below the threshold with near certainty. However, by the time of the 19^{th} June analysis, there is much greater flexibility and uncertainty in the evolution of R_t over time and correspondingly, after 3–4 weeks beyond the lock-down, R_t can no longer be said with certainty to be below 1. From this time there is an initial resurgence in the probability $R_t > 1$ which then plateaus from mid-May onwards. By the end of the period, there is the possibility that $R_t > 1$ in both the South West and in London, but it remains unlikely.

Table S4 gives the full estimation of the infection-fatality ratios only partially presented in Table 1.

Fig. S2 shows the goodness-of-fit to the death data by age, for each of the three post-lockdown analyses considered. In the 3^{rd} June analysis, there is a consistent under-estimation of the number of deaths from the beginning of May in the over–75s, with corresponding over-estimation in the younger age-groups. The model adaptation to allow for a different susceptibility to infection for the over-75s appears to rectify this lack of fit.

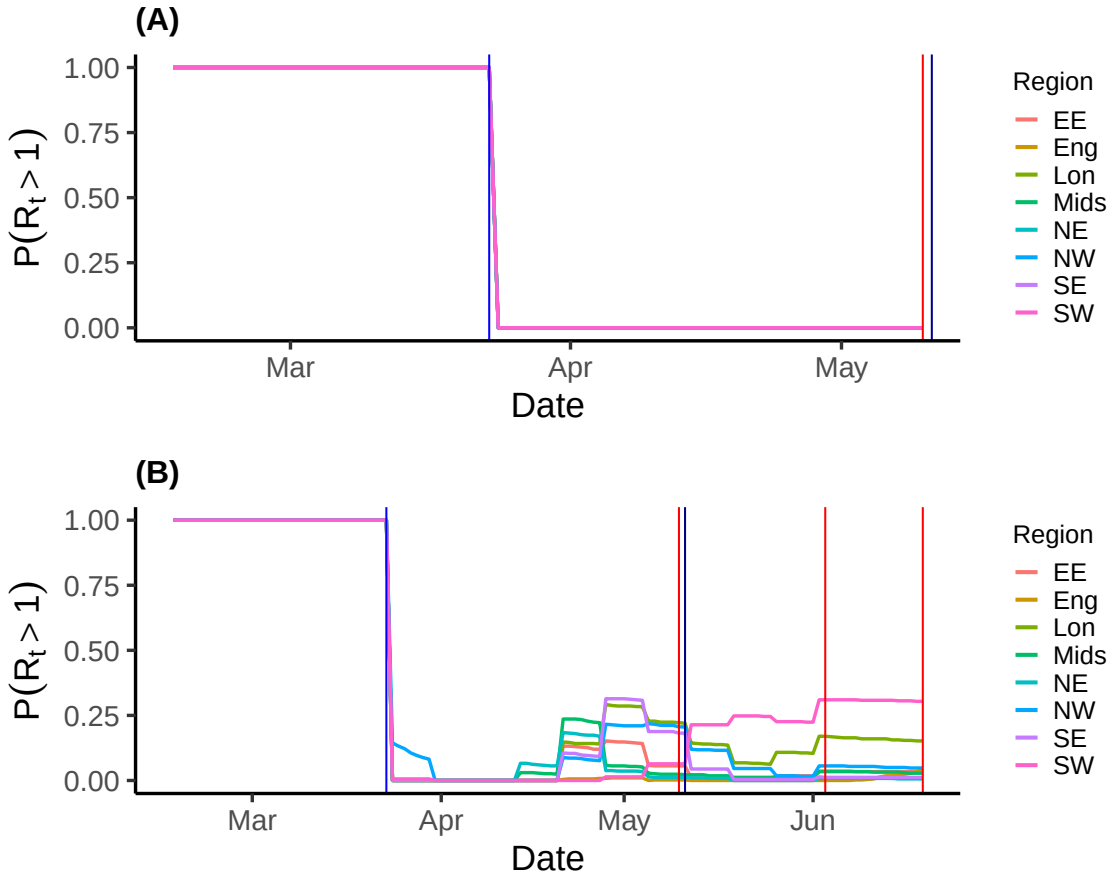

Figure S1: Equivalent plots to Fig. 3(B) for the analysis on (A) 10^{th} May, and (B) 19^{th} June.

Table S4: Estimates for the age-specific fatality ratio as they change over time

Age group (yrs)	10^{th} May	3^{rd} June	19^{th} June
< 5	0.0005% (0.00009%–0.0017%)	0.0004% (0.00002%–0.0016%)	0.0005% (0.00008%–0.002%)
5–14	0.0006% (0.0002%–0.0013%)	0.0010% (0.0005%–0.0018%)	0.0013% (0.0007%–0.0023%)
15–24	0.0032% (0.0019%–0.0049%)	0.0039% (0.0026%–0.0057%)	0.0043% (0.0029%–0.0062%)
25–44	0.018% (0.013%–0.024%)	0.024% (0.020%–0.029%)	0.029% (0.025%–0.034%)
45–64	0.28% (0.21%–0.37%)	0.36% (0.32%–0.42%)	0.44% (0.40%–0.49%)
65–74	1.8% (1.3%–2.3%)	2.3% (2.0%–2.7%)	2.9% (2.6%–3.2%)
> 74	16% (12%–21%)	23% (20%–27%)	17% (14%–22%)
Overall	0.63% (0.49%–0.81%)	0.88% (0.77%–1.0%)	17% (0.90%–1.4%)

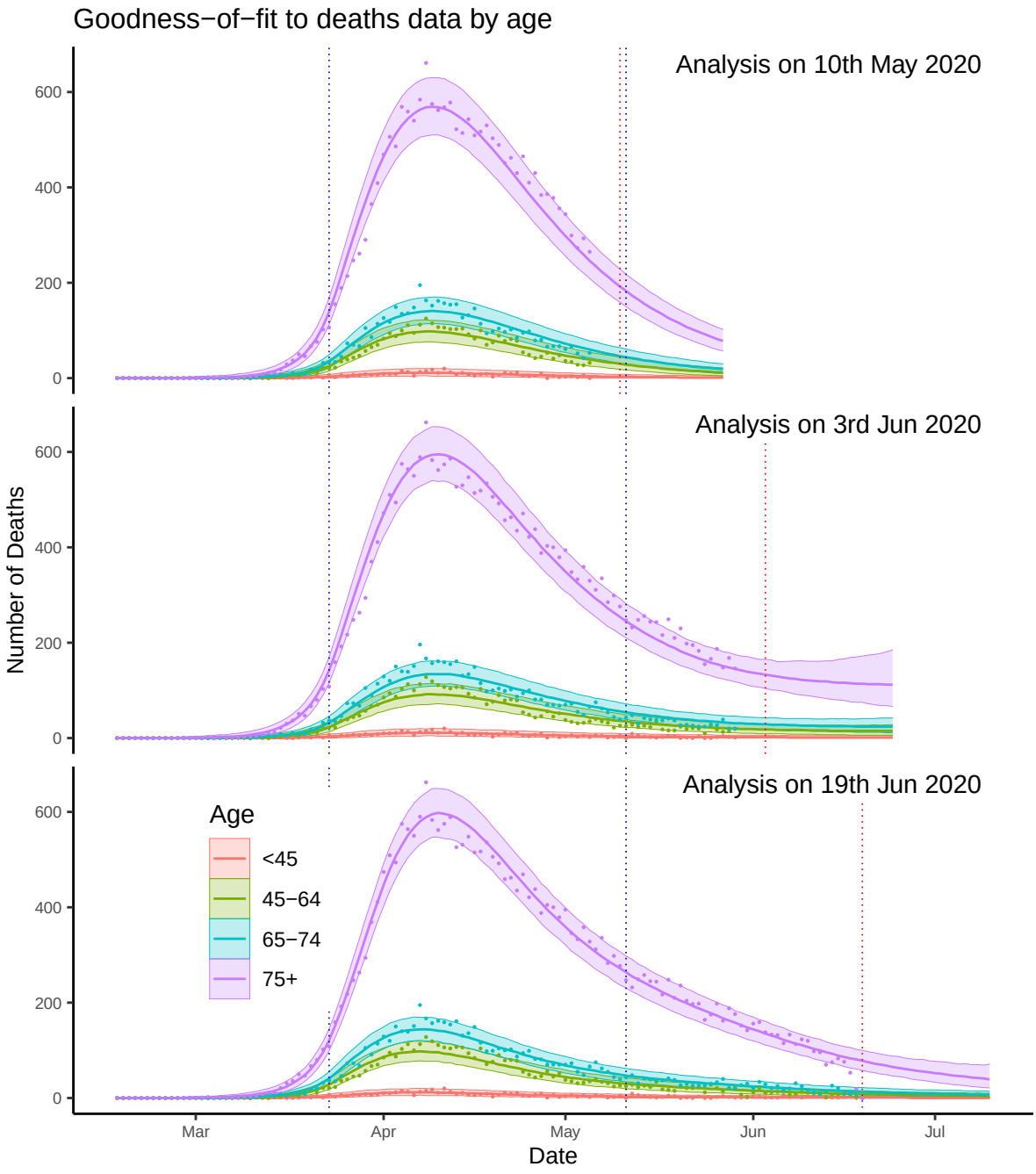

Figure S2: Goodness-of-fit to the deaths data by age on the 10^{th} May, 3^{th} June and 19^{th} June